* **Accepted Manuscript: Edwards, W. Brent, Ross H. Miller, and Timothy R. Derrick. "Femoral strain during walking predicted with muscle forces from static and dynamic optimization." Journal of biomechanics 49.7 (2016): 1206-1213.**

Original Manuscript

FEMORAL STRAIN DURING WALKING PREDICTED WITH MUSCLE FORCES FROM STATIC AND DYNAMIC OPTIMIZATION

W. Brent Edwards [a], Ross H. Miller [b], Timothy R. Derrick [c]

[a] Human Performance Laboratory
Faculty of Kinesiology
University of Calgary,
Calgary, AB T2N 1N4, CAN

[b] Department of Kinesiology
University of Maryland
College Park, MD 20745, USA

[c] Department of Kinesiology
Iowa State University
Ames, IA 50011, USA

Abstract word count: 250
Manuscript word count: 3860
Tables: 0
Figure: 7

Corresponding Author:
W. Brent Edwards, Ph.D.
Human Performance Laboratory
Faculty of Kinesiology
University of Calgary
KNB 418, 2500 University Dr. NW
Calgary, AB T2N 1N4
Phone: 403-220-2070
E-mail: wbedward@ucalgary.ca

ABSTRACT

Mechanical strain plays an important role in skeletal health, and the ability to accurately and noninvasively quantify bone strain *in vivo* may be used to develop preventive measures that improve bone quality and decrease fracture risk. A non-invasive estimation of bone strain requires combined musculoskeletal – finite element modeling, for which the applied muscle forces are usually obtained from static optimization (SO) methods. In this study, we compared finite element predicted femoral strains in walking using muscle forces obtained from SO to those obtained from forward dynamics (FD) simulation. The general trends in strain distributions were similar between FD and SO derived conditions and both agreed well with previously reported *in vivo* strain gage measurements. On the other hand, differences in peak maximum (ε_{max}) and minimum (ε_{min}) principal strain magnitudes were as high as 32% between FD ($\varepsilon_{max}/\varepsilon_{min}$ = 945/-1271 $\mu\varepsilon$) and SO ($\varepsilon_{max}/\varepsilon_{min}$ = 752/-859 $\mu\varepsilon$). These large differences in strain magnitudes were observed during the first half of stance, where SO predicted lower gluteal muscle forces and virtually no co-contraction of the hip adductors compared to FD. The importance of these results will likely depend on the purpose/application of the modeling procedure. If the goal is to obtain a generalized strain distribution for adaptive bone remodeling algorithms, then traditional SO is likely sufficient. In cases were strain magnitudes are critical, as is the case with fracture risk assessment, then bone strain estimation may benefit by including muscle activation and contractile dynamics in SO, or by using FD when practical.

KEYWORDS: biomechanics, bone, finite element model, mechanical loading, musculoskeletal model

INTRODUCTION

Bone is a dynamic tissue that exhibits a strong structure-function relationship with its mechanical loading environment. Indeed, physically active individuals tend to accrue more bone mass during growth and development, and better maintain this bone mass throughout adulthood, than their more sedentary counterparts (Parfitt, 1994). Additionally, the loss of ambulation and habitual muscle loading associated with bed rest or paralysis leads to a rapid and profound loss of bone mineral (Edwards et al., 2013a). In the complete absence of mechanical loading bone reverts to its genetic template, normal in shape and size but lacking distinct characteristics in trabecular microarchitecture, the amount of ossification, and thickness and curvature of the cortical diaphysis (Chalmers and Ray, 1962).

The process by which bone senses and responds to mechanical loading is known as functional adaptation, and the mechanical signal that drives this adaptive process is bone strain (Lanyon and Skerry, 2001), or some consequence thereof (i.e., strain energy density, fluid flow, microdamage). An accurate estimation of bone strain during activities of daily living such as walking is therefore integral to understanding the relationship between mechanical loading and skeletal health. In the physiological environment, bone strain is the end result of highly complex loading scenarios (i.e., combined axial, bending, shear, and torsional loading) caused by both gravitational and muscular forces. The resulting bone strain can be quantified *in vivo* using strain gages applied directly to the periosteal surface (Burr et al., 1996); however, the application of strain gages is highly invasive and measurements are limited to only a few, superficial locations. Owing to these limitations, researchers have turned to combined musculoskeletal – finite element modeling techniques for a more non-invasive estimation of bone strain (Anderson and Madigan, 2013; Speirs et al., 2007; Vahdati et al., 2014; Viceconti et al., 2012; Wagner et al., 2010).

The concurrent solving of musculoskeletal – finite element models is highly computationally intensive. Methods for estimating muscle forces from musculoskeletal models can require hundreds, thousands, or even millions of iterations within numerical optimization routines (Erdemir et al., 2007), and spending hours or even minutes within each iteration solving a finite element model would incur an impractical amount of computational time. As such, it is most common to use a post-processing technique whereby muscle forces derived from a higher-level rigid multibody simulation are used as boundary conditions for a lower-level elastic model to quantify bone strain (Anderson and Madigan, 2013; Speirs et al., 2007; Vahdati et al., 2014; Viceconti et al., 2012; Wagner et al., 2010). Inherent to a post-processing approach is the assumption that the underlying elastic deformation has no influence on the dynamics of the rigid multibody system. For the calculation of bone strain, this assumption is logical given that bone deformation (Burr et al., 1996) is orders of magnitude lower than that of the musculotendonous units (Fukunaga et al., 2001) and would theoretically have a negligible influence on whole-body motion.

The redundancy of the musculoskeletal system allows for an infinite number of muscle force combinations capable of producing the observed joint motions during physical activity (Crowninshield and Brand, 1981). This so-called “force-distribution problem” is typically overcome using numerical optimization procedures (Erdemir et al., 2007). For researchers using combined musculoskeletal – finite element modeling techniques, muscle forces are most frequently predicted using inverse dynamics-based static optimization (Anderson and Madigan, 2013; Speirs et al., 2007; Vahdati et al., 2014; Wagner et al., 2010). Static optimization is much less computationally intensive than dynamic optimization, which uses forward dynamics simulation to find optimal motions and controls for a given performance objective, such as tracking an experimental dataset and/or minimizing the metabolic energy expended. Although muscle forces from SO and FD have previously been deemed similar for walking (Anderson and Pandy, 2001b), SO has been criticized for lacking explicit time-dependent aspects of muscle force production, and for predicting minimal levels of antagonistic muscle co-contraction (Brand et al., 1994; Collins, 1995), which could potentially have a large influence on overall bone deformation and corresponding strain predictions.

The purpose of this study was to quantitatively evaluate finite element predicted periosteal strains at the femur during walking using muscle forces estimated from static and dynamic optimization. To this end, a previously described forward dynamics (FD) simulation of walking was performed using a 3D musculoskeletal model (Fig. 1), and intersegmental joint moments from FD were subsequently used in an inverse-dynamics-based static optimization (SO) routine. The muscle forces obtained from FD and SO served as post-possessing inputs to a finite element (FE) model of a femur based on clinical computed tomography (CT) data, and the resulting periosteal strains were compared between FD and SO derived conditions.

METHODS

Musculoskeletal modeling

A 3D musculoskeletal model (Fig. 1c) parameterized to represent a young adult female (i.e., 20 to 35 years) with standing height of 1.65 m and body mass of 61.0 kg was used to simulate walking at 1.25 m/s. The model was conceptually similar to other models used to perform FD gait simulations (Allen and Neptune, 2012; Anderson and Pandy, 2001a) and has been previously described in detail (Miller et al., 2015). Briefly, the model consisted of 10 rigid segments (pelvis, trunk, thighs, shanks, feet, toes) connected at nine joints actuated by 78 Hill-based muscle models (Fig. 1b), including 20 muscles per leg that crossed the hip and/or physically connected to the femur. Contact between the feet and the ground was modeled by an array of viscoelastic/Coulomb friction elements on the plantar surfaces of the feet and toe segments. Initial muscle parameters were referenced from a cadaver-based lower limb model (Arnold et al., 2010), which were then adjusted so that joint strength characteristics were similar to average dynamometry data for young adult females (Anderson et al., 2007).

Forward dynamics simulation. A simulation of one stride of periodic, bilaterally symmetric walking was performed using a dynamic optimization routine described in our previous work (Miller et al., 2012; Miller et al., 2015) and by others (Allen and Neptune, 2012; Umberger, 2010). Briefly, the muscle excitations were parameterized as bimodal signals with two magnitude and four timing parameters per muscle (Fig. 1a). The excitation parameters were optimized to track human experimental gait data (Miller et al., 2014). Specific gait variables included in the tracking cost function were average time series for the pelvis (3D), lumbar (3D), hip (3D), knee (1D), and ankle (1D) angles, the ground reaction force (3D), and the knee adduction moment. To discourage solutions that tracked these data with excessive energy expenditure, the metabolic energy per unit distance traveled was also calculated (Umberger et al., 2003) and added to the cost function (see Electronic Supplementary Material for details). A parallel simulated annealing algorithm (SPAN; (Higginson et al., 2005) was used to systematically adjust muscle excitation parameters so that the cost function was minimized (Fig. 1d). Muscle excitation timings for larger muscles were constrained to be similar to normative human electromyogram timing (Sutherland, 2001).

Inverse dynamics based static optimization. An inverse dynamics analysis was performed using data obtained from FD simulation to calculate the intersegmental joint forces and moments. The joint moments and muscle moment arms were used as inputs to a SO problem similar to our previous work (Edwards et al., 2010; Miller et al., 2014), which was solved using the interior-point algorithm in the Matlab Optimization Toolbox. At each time step of the simulated gait cycle, the muscle forces were determined such that (i) all joint moments from the inverse dynamics analysis were reproduced (equality constraint) and (ii) the sum of the squared muscle stresses was minimized (Glitsch and Baumann, 1997). This approach, which is conceptually similar to that of Anderson and Pandy (2001b), was chosen to eliminate differences between muscle forces from FD and SO associated with errors in the collection and processing of experimental data, and the estimation of segment anthropometry. All muscles were modeled as ideal force generators with no contractile or elastic properties because previous studies have suggested adjusting solution boundaries by activation dynamics has a negligible influence on muscle force predictions in walking (Anderson and Pandy, 2001b).

Finite element modeling

A FE model of a full femur was obtained from the VAKHUM database (http://www.ulb.ac.be/project/vakhum/). The native geometry and material properties of the model were based on clinical CT data from a female cadaver (age: 99 yrs, height: 155 cm, mass: 55 kg). The CT scan had acquisition setting of 120 kVp and 200 mAs, and images were reconstructed with a slice thickness of 2.7 mm and an in-plane pixel resolution of 0.840 mm. The FE model was comprised of 104,945 linear hexahedral elements with 115,835 degrees of freedom, corresponding to a nominal element edge length of 2.0 mm. Increasing element edge length from 2.0 to 3.0 mm changed femoral displacements, principal stresses, and principal strains by less than 3%, indicating adequate convergence at this refinement.

The FE model was first scaled longitudinally to the femoral body of the musculoskeletal model, and then scaled radially assuming bone mass scales to body mass, or length·diameter^2 $\propto$ body mass (McMahon, 1973), as further justified by the observed correlations between whole-body bone mineral content and body mass (Weiler et al., 2000). Elements were assigned to one of 283 linear-elastic material properties based on relationships between Hounsfield units and apparent density after the integral volumetric bone mineral density of the entire femur was increased by 26% to match that of a young adult female (Keaveny et al., 2010). The density-elasticity relationship was based on uniaxial mechanical testing data of femoral neck trabecular bone (Morgan et al., 2003):

$$E = 6850\rho_{app}^{1.49}$$

where E is the elastic modulus in MPa, and ρ_{app} is the apparent density in g/cm^3; all materials were assigned a Poisson's ratio of 0.3. These material property assignments have previously illustrated excellent agreement (r^2=0.91, RMSE<10%) between experimentally measured and FE-predicted principal strains for cadaveric proximal femora loaded in a stance configuration (Schileo et al., 2007).

An affine iterative-closest-point registration procedure available from Matlab Central File Exchange (http://www.mathworks.com/matlabcentral/fileexchange/24301-finite-iterative-closest-point) was used to align the FE and musculoskeletal model femur into a common local coordinate system. Femoral muscle insertion locations from the musculoskeletal model were then mapped to surface nodes of the FE model. Forces for each of the gluteal muscles (i.e., maximus, medius, and minimus) were equally distributed amongst three separate insertion locations, and the force for the adductor magnus muscle was equally distributed amongst four separate insertion locations (Arnold et al., 2010). The FE model was physiologically constrained at the lateral epicondyle, center of the patellar groove, and the femoral head contact point (Speirs et al., 2007). The hip joint contact force and muscle forces obtained from FD and SO at 10% increments of the gait cycle, from 0% to 100% of stance, as well as the instant of the 1st and 2nd peak resultant hip joint contact force (JCF1 and JCF2) served as boundary conditions for an implicit FE analysis (Fig. 1e), which was solved using Abaqus/Standard v6.13 (Dassault Systèmes Simulia Corp., Providence, RI). All forces were applied as point loads and resulting strain concentrations were removed from further analysis by discarding nodes and elements in the immediate vicinity of load application (Polgar et al., 2003).

Data reduction

The strains occurring along the periosteal surface of the proximal lateral aspect of the femur (35 mm distal to the lateral eminence of the greater trochanter) were compared between FD and SO derived conditions, simply because strains at this location have been directly measured *in vivo* (Aamodt et al., 1997). To replicate experimental measurement from a strain gage rosette, three-dimensional strains at this location were averaged over a 3 x 3 mm region and then transformed into a local coordinate system with a unit normal to the model exterior surface. The longitudinal (ε_{long}), transverse (ε_{trans}), and shear (ε_{shear}) planar strains occurring at this surface were calculated, as well as the maximum (ε_{max}) and minimum (ε_{min}) principal strains, and principal tensile strain (i.e., ε_{max}) angle. For a quantitative comparison of the global femoral strain distribution between FD and SO derived conditions, ε_{max} and ε_{min} occurring along four nodal paths at the anterior, lateral, posterior, and medial periosteal surface of the femoral shaft were quantified at the instant of JCF1 and JCF2.

RESULTS

The FD simulation walked at 1.25 m/s with a gross metabolic cost of 3.64 J/m/kg; kinematics and GRF were always within two standard deviations of the experimental means (Fig. 2). Differences in the hip joint contact forces were observed between FD and SO conditions, especially during the first 50% of stance (Fig. 3). While the resultant hip joint contact force at JCF1 was greater in FD than in SO (1824 vs. 1113 N, respectively), the resultant force at JCF2 was quite similar between conditions (1410 vs. 1406 N, respectively).

Examination of individual muscle forces suggested that the large differences in hip joint contact force during the first half of stance was primarily due to gluteal muscle force predictions, which were considerably lower for SO (Fig. 3). Despite these relatively large differences, the hip joint contact and muscle forces from FD and SO both produced femoral bending about an anteriomedial axis with the largest ε_{max} values observed along the lateral surface of the femoral shaft followed by the anterior surface, and the largest ε_{min} values observed along the medial surface followed by the posterior surface (Fig. 4). The unbalanced moments at the patellar groove associated with the physiologic constraints as well as error in the muscle mapping procedure were small and differed only slightly between FD and SO conditions (Fig. 5).

The strain predictions at the proximal lateral femur for both FD and SO illustrated a bimodal curve associated with the weight acceptance and push off phases of gait (Fig. 6). The largest differences in planar strains were observed at 30% of stance, near the instant of JCF1. At this point in the gait cycle, absolute values of ε_{long} and $\varepsilon_{trans,}$ were approximate 37% greater for FD, corresponding to a difference of 278 and 85 με, respectively. The absolute difference in ε_{shear} at this instant was 7 με, whereas ε_{max} and $\varepsilon_{min,}$ differed by approximate 36%, corresponding to 275 and 84 με, respectively. Differences in principal strain angle were never greater than 5˚.

The largest differences in the strain distribution across the length of the femur were observed at JCF1 along the lateral and medial boarders of the femoral shaft (Fig. 7). Peak ε_{max} at JCF1 differed by approximately 250 με along the lateral surface and peak ε_{min} by 412 με along the medial surface; differences in peak ε_{max} and ε_{min} along the anterior and posterior surfaces were relatively small (≤ 113 με). Peak ε_{max} at JCF2 differed by approximately 100 με along the lateral surface and peak ε_{min} by 119 με along the medial surface. The difference in peak ε_{max} along the anterior surface was 42 με, while that for peak ε_{min} along the posterior surface was 171 με.

DISCUSSION

Mechanical strain plays an important role in skeletal health, and the ability to accurately and non-invasively quantify bone strain *in vivo* may be used to develop preventive measures that improve bone quality and decrease fracture risk. Our purpose was to compare FE predicted femoral strains during the stance phase of walking using muscles forces obtained from FD simulation and inverse-dynamics-based SO. Despite having identical joint kinematics and intersegmental reaction forces and moments, differences as high as 32% were observed in peak femoral principal strains between FD and SO derived conditions (-1271 με vs. -859 με, respectively). The importance of these differences will likely depend on the purpose/application of the combined musculoskeletal – finite element modeling procedure.

The muscle force predictions generated by both FD and SO produced femoral bending about an anteriomedial axis with the highest principal tensile strains along the lateral and anterior surface of the femur, and the highest principal compressive strains along the medial and posterior surface of the femur. These global strain distributions are quite similar to those previously reported for FE models loaded with physiological boundary conditions simulating gait (Anderson and Madigan, 2013; Duda et al., 1998; Polgar et al., 2003; Speirs et al., 2007; Wagner et al., 2010). Both FD and SO muscle forces generated peak principal tensile strains and peak principal compressive strains on the order of 500 to 1000 με, and -1000 to -1500 με, respectively. These strain magnitudes agree well with previous literature (Duda et al., 1998; Polgar et al., 2003), but in some circumstances are 2-3 times lower (Anderson and Madigan, 2013; Speirs et al., 2007; Wagner et al., 2010). Although some of the discrepancy in strain magnitudes may be associated with specific details of the musculoskeletal model geometry and procedures, they could just as easily be explained by differences in the calculated/assumed bone mineral density distribution of the femur or material property assignment for the FE model. Near twofold differences in predicted strain magnitudes have been reported between some of the most commonly utilized density-elasticity relationships for FE models of bone (Schileo et al., 2007). Nevertheless, it is important to note that the strain magnitudes observed herein are directly in line with previous *in vivo* measurements (Aamodt et al., 1997; Burr et al., 1996).

Strain gage measurements during walking have been recorded at the proximal lateral femur in a 49-year-old female undergoing surgery for “snapping hip syndrome” (Aamodt et al., 1997). The strain gage recordings demonstrated that the proximal lateral femur was undergoing tension during the stance phase of gait. The axial strain along the longitudinal axes of the femur reached 1,133 $\mu\varepsilon$, with an ε_{max} to ε_{min} ratio of -3.05 (1,198/-393 $\mu\varepsilon$), and an average principal tensile strain angle 12˚ from the longitudinal axis of the femur. The axial strains along the longitudinal axes of the femur for FD reached 745 $\mu\varepsilon$ near JCF1, and displayed an ε_{max} to ε_{min} ratio of -3.25 (747/-230 $\mu\varepsilon$); corresponding values for SO near JCF1 were: axial strain = 467 $\mu\varepsilon$, and ε_{max} to ε_{min} ratio=-3.22 (471/-146 $\mu\varepsilon$). The average principal tensile strain angle from the longitudinal axis of the femur during stance was 6.5˚ (range: -6.0 to 20.6˚) for FD and 5.7˚ (range: -7.3 to 18.8˚) for SO. Use of these strain gage data for a rigorous validation of the two modeling procedures employed herein would be a futile exercise, as there are simply too many differences (e.g., age, femoral geometry) and unknowns (e.g., normalcy of gait mechanics following surgery, walking speed, exact location of strain gage) associated with the experimental data. In fact, changing the simulated strain gage location only a few millimeters anterior or inferior increased strain magnitudes by 100 to 200 με. What is important to note is that the general trends in strain for both methods, such as the tension-compression ratio and orientation of the principal axis, seem to correspond with the experimental data.

The largest differences in femoral strains between FD and SO were observed during the first half of stance, where SO predicted much lower gluteal muscle forces and virtually no co-contraction of the hip adductors compared to FD. This reduction in muscle co-contraction of the frontal plane hip agonists and antagonist has recently been suggested as a potential cause of lower hip contact force predictions using static optimization when compared to computed muscle control for FD simulation (Wesseling et al., 2015). In this study, differences in muscle forces produced strains that were some 30% lower along the lateral and medial surface using SO. On the other hand, peak strain along the anterior surface at JCF1 was higher using SO by nearly 113 με. Although joint contact forces were similar between conditions at JCF2, differences in strain distributions up to 171 με were still observed, demonstrating that the relationship between applied load and resulting bone strain is quite complex. A general limitation of this study is that we cannot affirm which method of muscle force estimation is more accurate. Confirmation of accuracy would require *in vivo* measurements of muscle forces thereby negating a musculoskeletal modeling exercise all together. However, practical non-invasive measurements of *in vivo* muscle forces is unlikely to be realized in the near future, and there remains a need to grow the knowledge base of "best practices" for modeling these aspects of human movement (Hicks et al., 2015). Although FD does not necessarily predict more realistic muscle forces than SO, it does allow for the prediction of forces that are associated with physiologically-motivated objectives (e.g. the propensity to minimize metabolic cost; Srinivasan, 2009) that cannot be included explicitly in SO, and can assess how modeling methods and assumptions may affect the outcomes of simulation studies (Anderson and Pandy, 2001b; Morrow et al., 2014).

This study has several limitations that should be borne in mind for the general interpretation and future investigation of combined musculoskeletal – finite element modeling for the non-invasive assessment of bone strain. Although the FE model was modified to have similar size and density to that of a young adult female, the gross morphology and mineral distribution of the model was based on a 99 year-old cadaver. In aging, there is a progressive thinning of the cortical shell (Thompson, 1980) and a reduction in femoral neck shaft angle (Rickels et al., 2011). In fact, the femoral neck shaft angle was approximately 5˚ lower for the FE model compared to the musculoskeletal model. While these differences may have influenced the absolute values of strain, we have no reason to think that the relative differences between conditions, and thus the interpretation of our findings, would change. This study design allowed for a direct comparison of FD and SO in the absence of experimental error (Anderson and Pandy, 2001b). The FD simulation represented only one ensemble average stride of walking, and we can say nothing of the variability of bone strain between strides or different levels of co-contraction. Future work may examine the importance of this variability through stochastic representation of neuromuscular control (Martelli et al., 2015; Viceconti et al., 2012).

The FE method is perhaps the most accurate of all current biomechanical modeling approaches because their outputs can be directly compared to *in vitro* experiments (Edwards et al., 2013b; Schileo et al., 2007). Although notably difficult, more work is needed to validate muscle outputs from musculoskeletal models, recognizing that until such time, bone strain predictions based on combined musculoskeletal – finite element modeling may lead to erroneous conclusions regarding bone factor of safety and remodeling stimuli. If the goal of the modeling procedure is to obtain a generalized strain distribution for adaptive bone remodeling algorithms (Vahdati et al., 2014) both static and dynamic methods should produce analogous results, provided that stimulus thresholds are adjusted accordingly. In circumstances were strain magnitudes are critical, as is the case with fracture risk assessment (Viceconti et al., 2012), it is possible that these two methods may lead to conflicting conclusions; fatigue-life predictions could potentially differ by one to two orders of magnitude (Carter and Caler, 1985). Performing FD will not always be practical due to the level of modeling and computational effort required, but in these situations, SO routines may benefit by including aspects of muscle force estimation from FD, as is done with methods like computed muscle control (Thelen and Anderson, 2006).

ACKNOWLEDGMENTS

This work was partly funded by the Natural Science and Engineering Research Council of Canada (RGPIN 01029-2015).

CONFLICT OF INTEREST STATEMENT

None of the authors have any conflicts of interest to disclose.

REFERENCES

Aamodt, A., Lund-Larsen, J., Eine, J., Andersen, E., Benum, P., Husby, O. S., 1997. In vivo measurements show tensile axial strain in the proximal lateral aspect of the human femur. Journal of Orthopaedic Research 15, 927-931.

Allen, J. L., Neptune, R. R., 2012. Three-dimensional modular control of human walking. Journal of Biomechanics 45, 2157-2163.

Anderson, D. E., Madigan, M. L., 2013. Effects of age-related differences in femoral loading and bone mineral density on strains in the proximal femur during controlled walking. Journal of Applied Biomechanics 29, 505-516.

Anderson, D. E., Madigan, M. L., Nussbaum, M. A., 2007. Maximum voluntary joint torque as a function of joint angle and angular velocity: model development and application to the lower limb. Journal of Biomechanics 40, 3105-3113.

Anderson, F. C., Pandy, M. G., 2001a. Dynamic optimization of human walking. Journal of Biomechanical Engineering 123, 381-390.

Anderson, F. C., Pandy, M. G., 2001b. Static and dynamic optimization solutions for gait are practically equivalent. Journal of Biomechanics 34, 153-161.

Arnold, E. M., Ward, S. R., Lieber, R. L., Delp, S. L., 2010. A model of the lower limb for analysis of human movement. Annals of Biomedical Engineering 38, 269-279.

Brand, R. A., Pedersen, D. R., Davy, D. T., Kotzar, G. M., Heiple, K. G., Goldberg, V. M., 1994. Comparison of hip force calculations and measurements in the same patient. The Journal of Arthroplasty 9, 45-51.

Burr, D. B., Milgrom, C., Fyhrie, D., Forwood, M., Nyska, M., Finestone, A., Hoshaw, S., Saiag, E., Simkin, A., 1996. In vivo measurement of human tibial strains during vigorous activity. Bone 18, 405-410.

Carter, D. R., Caler, W. E., 1985. A cumulative damage model for bone fracture. Journal of Orthopaedic Research 3, 84-90.

Chalmers, J., Ray, R. D., 1962. The groth of transplanted foetal bones in difference immunological environments. The Journal of Bone and Joint Surgery (Br) 44, 149-164.

Collins, J. J., 1995. The redundant nature of locomotor optimization laws. Journal of Biomechanics 28, 251-267.

Crowninshield, R. D., Brand, R. A., 1981. The prediction of forces in joint structures; distribution of intersegmental resultants. Exercise and Sport Sciences Reviews 9, 159-181.

Duda, G. N., Heller, M., Albinger, J., Schulz, O., Schneider, E., Claes, L., 1998. Influence of muscle forces on femoral strain distribution. Journal of Biomechanics 31, 841-846.

Edwards, W. B., Schnitzer, T. J., Troy, K. L., 2013a. Bone mineral loss at the proximal femur in acute spinal cord injury. Osteoporosis International 24, 2461-2469.

Edwards, W. B., Schnitzer, T. J., Troy, K. L., 2013b. Torsional stiffness and strength of the proximal tibia are better predicted by finite element models than DXA or QCT. Journal of Biomechanics 46, 1655-1662.

Edwards, W. B., Taylor, D., Rudolphi, T. J., Gillette, J. C., Derrick, T. R., 2010. Effects of running speed on a probabilistic stress fracture model. Clinical Biomechanics 25, 372-377.

Erdemir, A., McLean, S., Herzog, W., van den Bogert, A. J., 2007. Model-based estimation of muscle forces exerted during movements. Clinical Biomechanics 22, 131-154.

Fukunaga, T., Kubo, K., Kawakami, Y., Fukashiro, S., Kanehisa, H., Maganaris, C. N., 2001. In vivo behaviour of human muscle tendon during walking. Proceedings of the Royal Society of London. Series B, Biological Sciences 268, 229-233.

Glitsch, U., Baumann, W., 1997. The three-dimensional determination of internal loads in the lower extremity. Journal of Biomechanics 30, 1123-1131.

Hicks, J. L., Uchida, T. K., Seth, A., Rajagopal, A., Delp, S. L., 2015. Is my model good enough? Best practices for verification and validation of musculoskeletal models and simulations of movement. Journal of Biomechanical Engineering 137, 020905.

Higginson, J. S., Neptune, R. R., Anderson, F. C., 2005. Simulated parallel annealing within a neighborhood for optimization of biomechanical systems. Journal of Biomechanics 38, 1938-1942.

Keaveny, T. M., Kopperdahl, D. L., Melton, L. J.,3rd, Hoffmann, P. F., Amin, S., Riggs, B. L., Khosla, S., 2010. Age-dependence of femoral strength in white women and men. Journal of Bone and Mineral Research 25, 994-1001.

Lanyon, L., Skerry, T., 2001. Postmenopausal osteoporosis as a failure of bone's adaptation to functional loading: a hypothesis. Journal of Bone and Mineral Research 16, 1937-1947.

Martelli, S., Calvetti, D., Somersalo, E., Viceconti, M., 2015. Stochastic modelling of muscle recruitment during activity. Interface Focus 5, 20140094.

McMahon, T., 1973. Size and shape in biology. Science 179, 1201-1204.

Miller, R. H., Edwards, W. B., Brandon, S. C., Morton, A. M., Deluzio, K. J., 2014. Why don't most runners get knee osteoarthritis? A case for per-unit-distance loads. Medicine and Science in Sports and Exercise 46, 572-579.

Miller, R. H., Esterson, A. Y., Shim, J. K., 2015. Joint contact forces when minimizing the external knee adduction moment by gait modification: A computer simulation study. The Knee 22, 481-489.

Miller, R. H., Umberger, B. R., Hamill, J., Caldwell, G. E., 2012. Evaluation of the minimum energy hypothesis and other potential optimality criteria for human running. Proceedings of the Royal Society of London. Series B, Biological Sciences 279, 1498-1505.

Morgan, E. F., Bayraktar, H. H., Keaveny, T. M., 2003. Trabecular bone modulus-density relationships depend on anatomic site. Journal of Biomechanics 36, 897-904.

Morrow, M. M., Rankin, J. W., Neptune, R. R., Kaufman, K. R., 2014. A comparison of static and dynamic optimization muscle force predictions during wheelchair propulsion. Journal of Biomechanics 47, 3459-3465.

Parfitt, A. M., 1994. The two faces of growth: benefits and risks to bone integrity. Osteoporosis International 4, 382-398.

Polgar, K., Gill, H. S., Viceconti, M., Murray, D. W., O'Connor, J. J., 2003. Strain distribution within the human femur due to physiological and simplified loading: finite element analysis using the muscle standardized femur model. Proceedings of the Institution of Mechanical Engineers.Part H, Journal of Engineering in Medicine 217, 173-189.

Rickels, T., Kreuzer, S., Lovell, T., Nogler, M., Puri, L., 2011. Age and gender related differences in femoral neck - shaft angles. In Proceedings of the Orthopaedic Research Society 57th Annual Meeting, Long Beach, California. (http://www.ors.org/Transactions/57/2279.pdf)

Schileo, E., Taddei, F., Malandrino, A., Cristofolini, L., Viceconti, M., 2007. Subject-specific finite element models can accurately predict strain levels in long bones. Journal of Biomechanics 40, 2982-2989.

Speirs, A. D., Heller, M. O., Duda, G. N., Taylor, W. R., 2007. Physiologically based boundary conditions in finite element modelling. Journal of Biomechanics 40, 2318-2323.

Srinivasan, M., 2009. Optimal speeds for walking and running, and walking on a moving walkway. Chaos 19, 026112.

Sutherland, D. H., 2001. The evolution of clinical gait analysis part l: kinesiological EMG. Gait & Posture 14, 61-70.

Thelen, D. G., Anderson, F. C., 2006. Using computed muscle control to generate forward dynamic simulations of human walking from experimental data. Journal of Biomechanics 39, 1107-1115.

Thompson, D. D., 1980. Age changes in bone mineralization, cortical thickness, and haversian canal area. Calcified Tissue International 31, 5-11.

Umberger, B. R., 2010. Stance and swing phase costs in human walking. Journal of the Royal Society, Interface 7, 1329-1340.

Umberger, B. R., Gerritsen, K. G., Martin, P. E., 2003. A model of human muscle energy expenditure. Computer Methods in Biomechanics and Biomedical Engineering 6, 99-111.

Vahdati, A., Walscharts, S., Jonkers, I., Garcia-Aznar, J. M., Vander Sloten, J., van Lenthe, G. H., 2014. Role of subject-specific musculoskeletal loading on the prediction of bone density distribution in the proximal femur. Journal of the Mechanical Behavior of Biomedical Materials 30, 244-252.

Viceconti, M., Taddei, F., Cristofolini, L., Martelli, S., Falcinelli, C., Schileo, E., 2012. Are spontaneous fractures possible? An example of clinical application for personalised, multiscale neuro-musculo-skeletal modelling. Journal of Biomechanics 45, 421-426.

Wagner, D. W., Divringi, K., Ozcan, C., Grujicic, M., Pandurangan, B., Grujicic, A., 2010. Combined musculoskeletal dynamics/structural finite element analysis of femur physiological loads during walking. Multidiscipline Modeling in Materials and Structures 6, 417-437.

Weiler, H. A., Janzen, L., Green, K., Grabowski, J., Seshia, M. M., Yuen, K. C., 2000. Percent body fat and bone mass in healthy Canadian females 10 to 19 years of age. Bone 27, 203-207.

Wesseling, M., Derikx, L. C., de Groote, F., Bartels, W., Meyer, C., Verdonschot, N., Jonkers, I., 2015. Muscle optimization techniques impact the magnitude of calculated hip joint contact forces. Journal of Orthopaedic Research 33, 430-438.

FIGURE CAPTIONS

Figure 1. Diagram of the combined musculoskeletal – finite element modeling approach for FD simulation. (a) Muscle excitations are defined by six parameters per muscle: two values each for M_i, T_i^{on}, and T_i^{off}. (b) Each of the 78 muscles receives an excitation defined by its six muscle-specific parameters, and develops force in response. (c) Joint moments resulting from muscle forces are applied to the skeleton to cause motion. (d) Excitations are adjusted through optimization to minimize a cost function J. (e) Following optimization, the hip joint contact force and forces for muscles attaching to the femur are used as boundary conditions for a finite element model.

Figure 2. Lumbar, pelvis, and lower limb joint angles and ground reaction forces (GRF) for the FD simulation of walking. Shaded areas are ±2 standard deviations around the mean for 14 human subjects walking in a “normal and comfortable” fashion (Miller et al., 2014). The stride begins and ends at heel-strike. Vertical dashed lines indicate toe-off. The GRF are scaled by bodyweight (BW).

Figure 3. The resultant hip joint contact force and select muscle forces acting at the femur during the stance phase of gait (GMAX=gluteus maximus, GMED=gluteus medius, GMIN=gluteus minimus, ADDMAG=adductor magnus, RECFEM=rectus femoris, VAS = vasti muscles, HAM=hamstring muscles, GAS = gastrocnemius). The hip joint contact force was calculated as the vector sum of the resultant joint reaction force and the forces from muscles spanning the hip.

Figure 4. The minimum principal strain (ε_{min}) distribution on the medial surface (left) and maximum principal strain (ε_{max}) distribution on the lateral surface (right) at JCF1.

Figure 5. The unbalanced moments, or reaction moments, at the distal patellar groove associated with the physiological constraints as well as error in the muscle mapping procedure.

Figure 6. The longitudinal (ε_{long}), transverse (ε_{trans}), and shear (ε_{shear}) planar strains, as well as the maximum (ε_{max}) and minimum (ε_{min}) principal strains, and principal tensile strain (i.e., ε_{max}) angle occurring at the proximal lateral femur (35 mm distal to the lateral eminence of the greater trochanter) as a function of stance.

Figure 7. The maximum principal strains (ε_{max}) along nodal paths of the lateral and anterior surfaces, and minimum principal strains (ε_{min}) along nodal paths of the medial and posterior surfaces at JCF1 (top) and JCF2 (bottom).

FIGURES

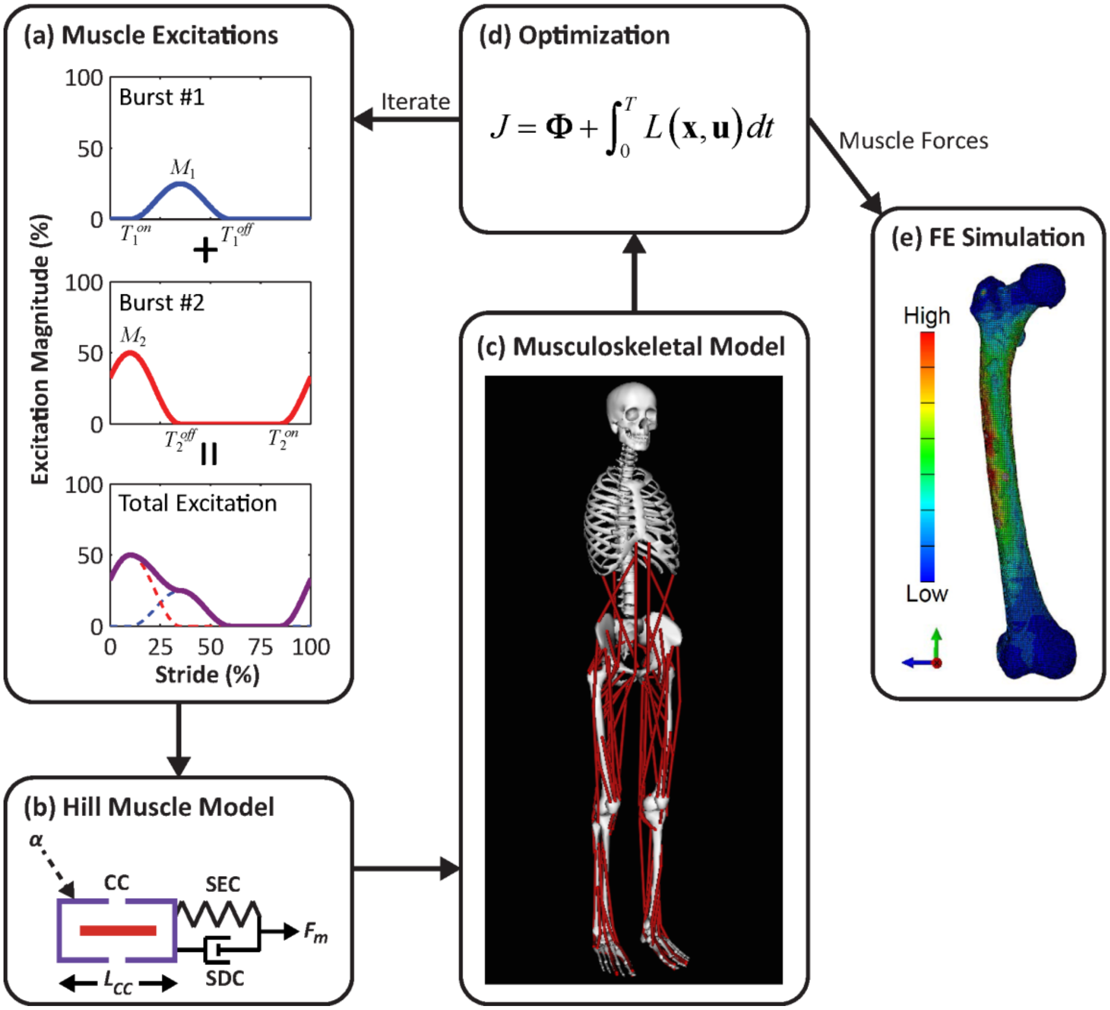

Figure 1.

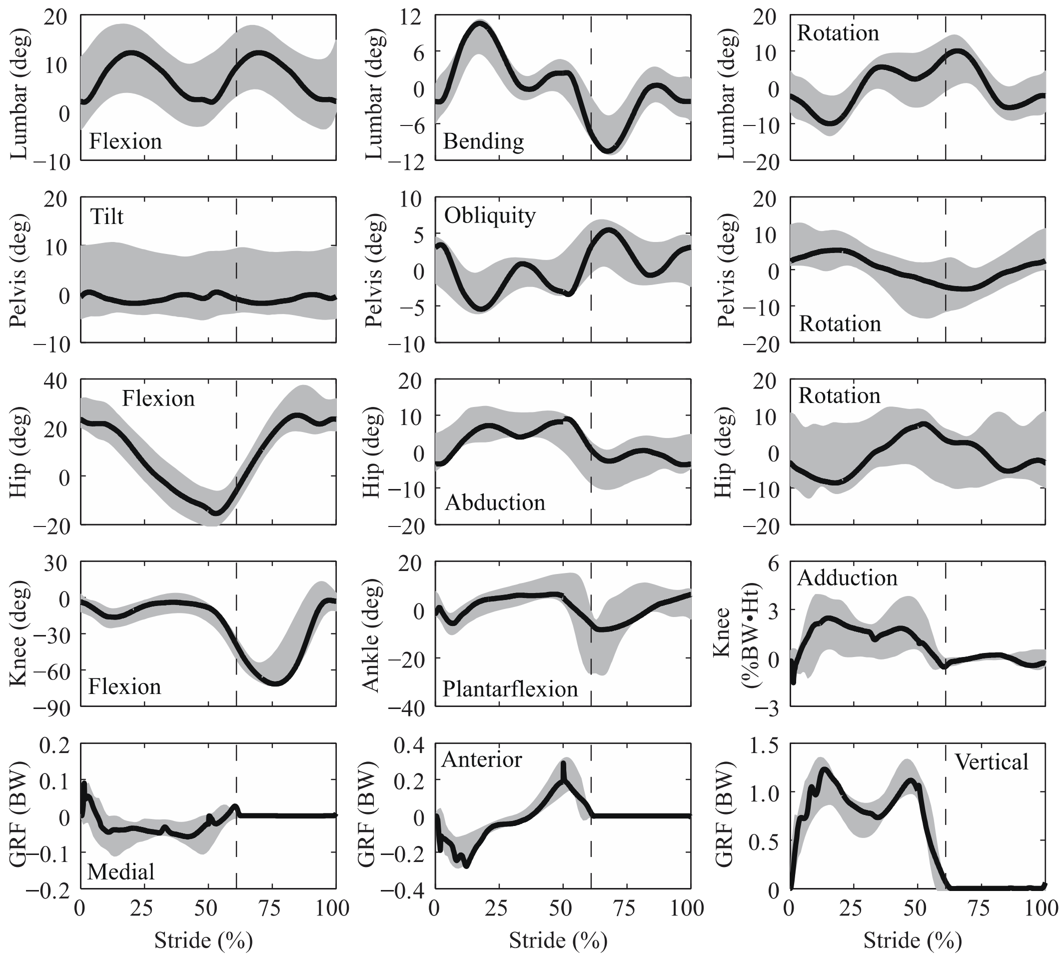

Lumbar (deg)
Flexion
Bending
Rotation
Pelvis (deg)
Tilt
Obliquity
Rotation
Hip (deg)
Flexion
Abduction
Rotation
Knee (deg)
Flexion
Ankle (deg)
Plantarflexion
Knee (%BW•Ht)
Adduction
GRF (BW)
Medial
Anterior
Vertical
Stride (%)

Figure 2.

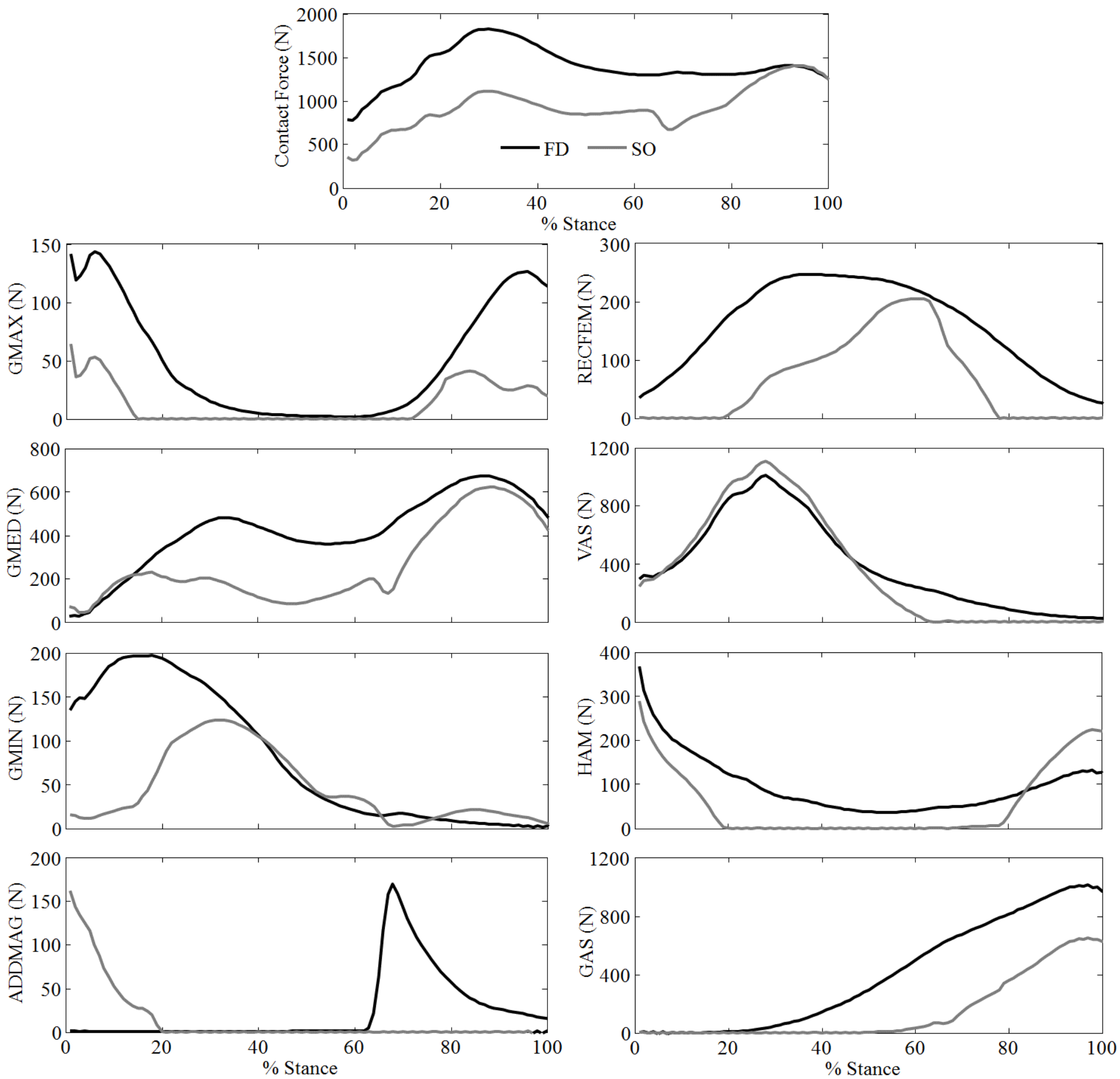
Contact Force (N)
% Stance
FD
SO
GMAX (N)
RECFEM (N)
GMED (N)
VAS (N)
GMIN (N)
HAM (N)
ADDMAG (N)
GAS (N)
% Stance
% Stance

Figure 3.

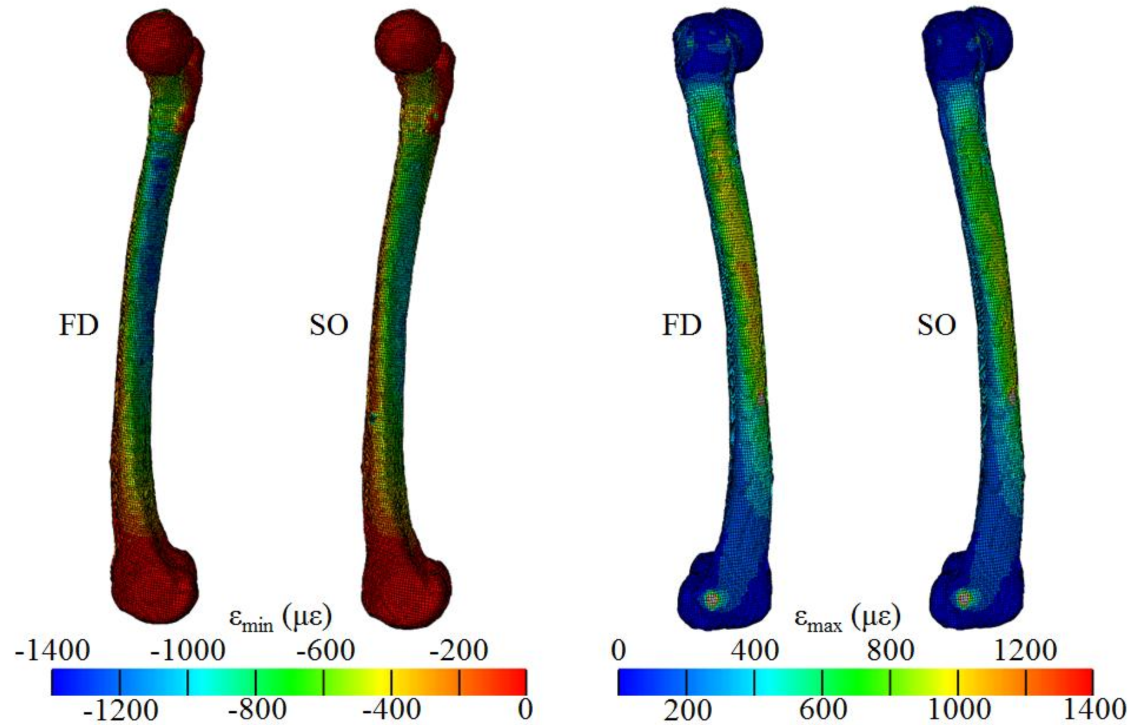
FD
SO
FD
SO
εmin (με)
-1400
-1000
-600
-200
-1200
-800
-400
0
εmax (με)
0
400
800
1200
200
600
1000
1400

Figure 4.

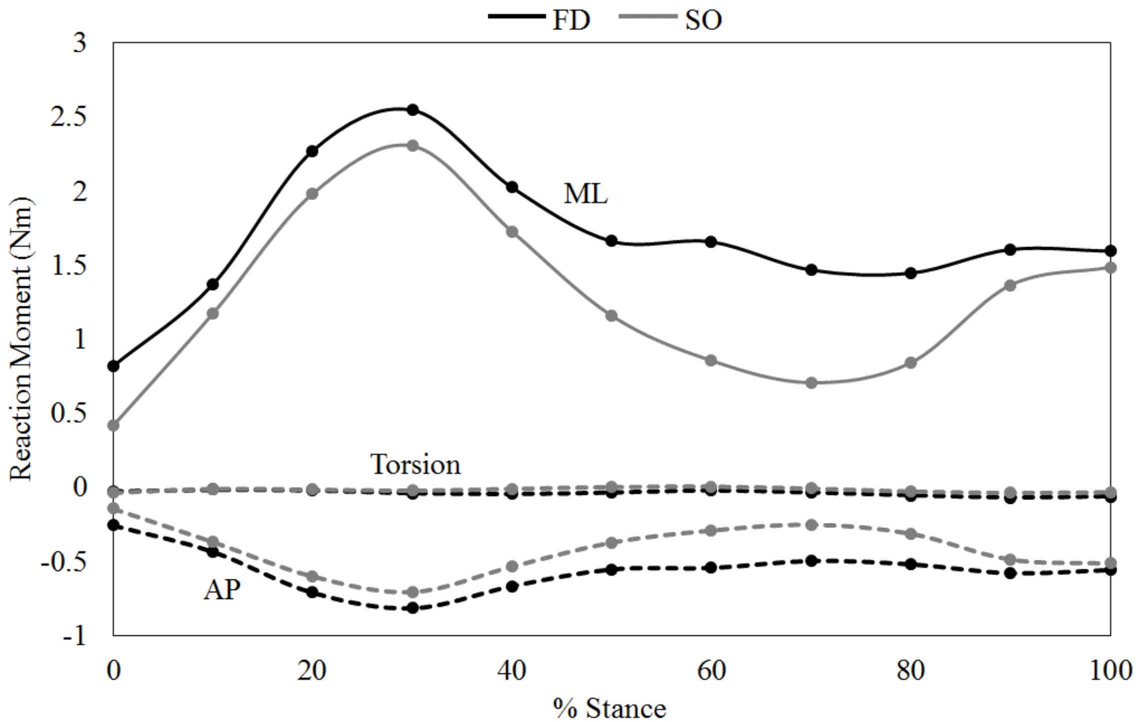
FD
SO
Reaction Moment (Nm)
3
2.5
2
1.5
1
0.5
0
-0.5
-1
ML
Torsion
AP
0
20
40
60
80
100
% Stance

Figure 5.

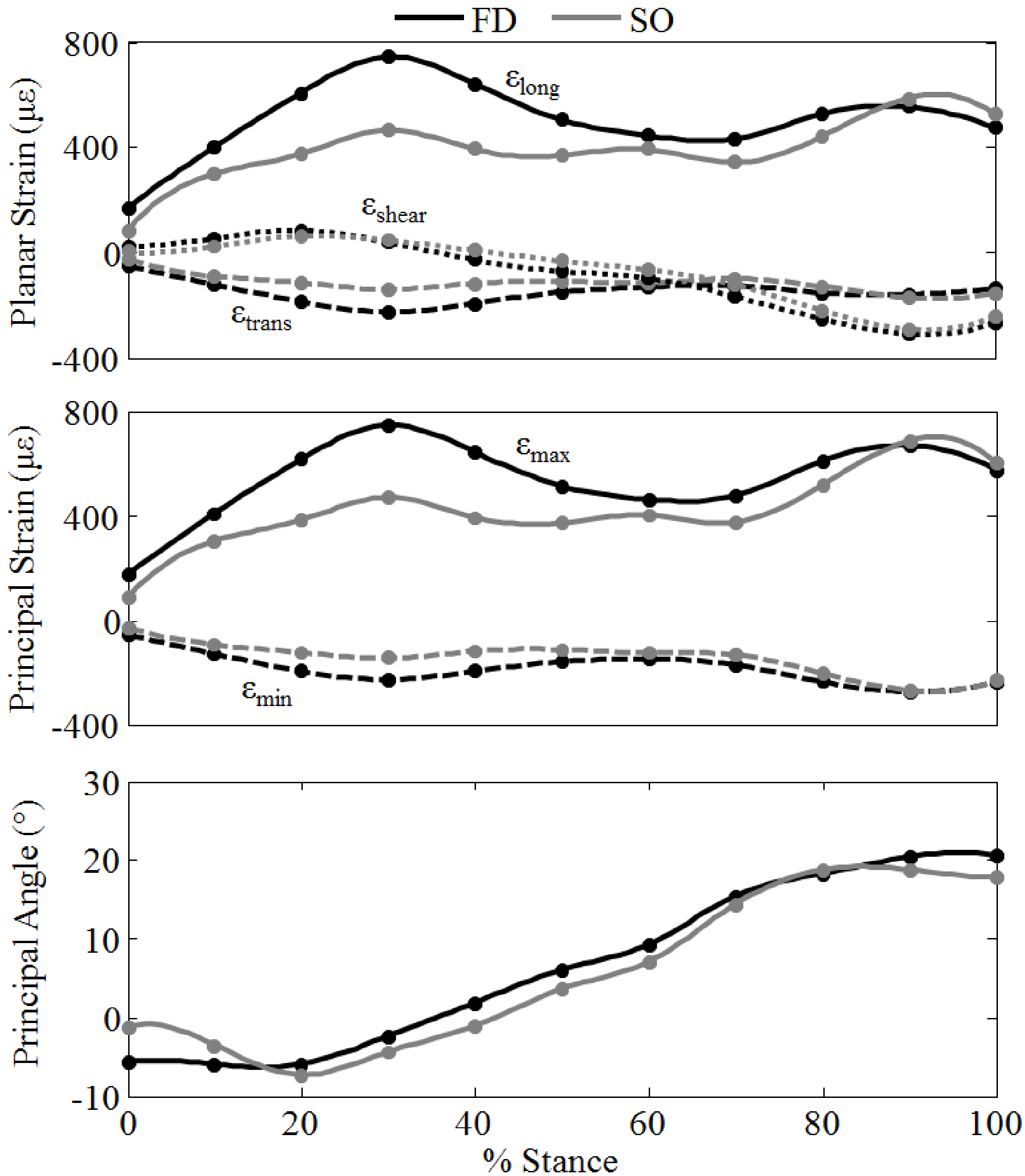

FD
SO
800
400
0
-400
Planar Strain (με)
ε_long
ε_shear
ε_trans
800
400
0
-400
Principal Strain (με)
ε_max
ε_min
30
20
10
0
-10
Principal Angle (°)
0
20
40
60
80
100
% Stance

Figure 6.

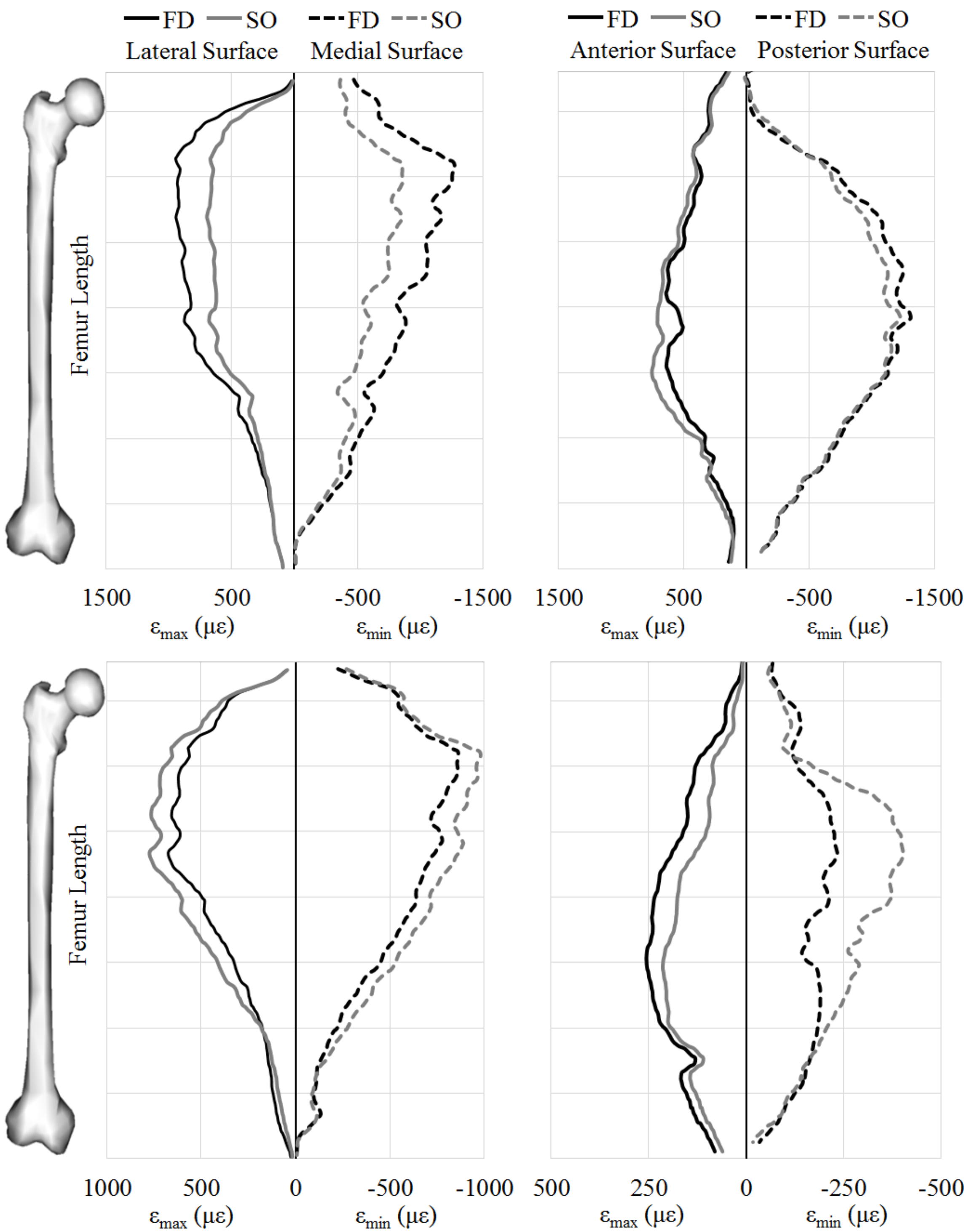

FD
SO
FD
SO
Lateral Surface
Medial Surface
FD
SO
FD
SO
Anterior Surface
Posterior Surface
Femur Length
1500
500
-500
-1500
ε_{max} (με)
ε_{min} (με)
1000
500
0
-500
-1000
500
250
0
-250
-500

Figure 7.

Electronic Supplementary Material

Femoral strain during walking predicted with muscle forces from static and dynamic optimization

W. Brent Edwards [a], Ross H. Miller [b], Timothy R. Derrick [c]

[a] Human Performance Laboratory
Faculty of Kinesiology
University of Calgary,
Calgary, AB T2N 1N4, CAN

[b] Department of Kinesiology
University of Maryland
College Park, MD 20745, USA

[c] Department of Kinesiology
Iowa State University
Ames, IA 50011, USA

*Corresponding author at: KNB 418, 2500 University Dr. NW, Calgary, AB T2N 1N4. Phone: 403-220-2070. E-mail: wbedward@ucalgary.ca (W. Brent Edwards).

Cost Function for Forward Dynamics Simulation

The cost function for the forward dynamics simulation was (Miller et al., 2015):

$$J = J_{track} + w_1 J_{metcost} + w_2 J_{exc}$$

where J_{track} is the mean squared deviation from the target data, $J_{metcost}$ is the square of the gross metabolic cost of transport (Tucker, 1975), J_{exc} is deviations in the on/off timing of the model's muscle excitations relative to normal human electromyograms (EMG), and w_1 *and* w_2 are weighting coefficients. The specific form of the tracking function was:

$$J_{track} = \frac{1}{15T} \sum_{i=1}^{15} \left(\int_0^T \left(\frac{x_i^{mod}(t) - x_i^{tar}(t)}{w_i^{tar}(t)} \right)^2 dt \right)$$

where $x_i^{mod}(t)$ is the value of variable *i* at time *t* from the model, $x_i^{tar}(t)$ is the value of the analogous tracking target variable, $w_i^{tar}(t)$ is a weighting factor, and T is the step duration. We used means and between-subjects standard deviations for "normal" human walking data from

Miller et al. (2014) to define $x_i^{tar}(t)$ and $w_i^{tar}(t)$, respectively. The 15 tracking targets included the 3D pelvis angles, the 3D lumbar joint angles, the 3D hip angles, the knee flexion angle, the ankle plantarflexion angle, the 3D ground reaction force, and the knee adduction moment.

The specific form of the metabolic cost function was:

$$J_{metcost}=\left(\frac{\int_0^{\mathrm{T}}\left(\dot{E}_{rest}+\sum_{m=1}^{78}\dot{E}_m\right)dt}{v_{avg}TM}\right)^2$$

where $\dot{E}_{rest}$ is the resting metabolic rate, chosen to be 1.0 W/kg body mass (Waters & Mulroy, 1999), $\dot{E}_m$ is the gross metabolic rate of muscle m, calculated using the Umberger et al. (2003) model of human muscle energy expenditure for Hill-based muscle models, v_{avg} is the average horizontal speed of the model's center of mass during $t \in [0,T]$, and M is the total body mass. The value of the weighting coefficient $w_1 = 0.2$ was chosen so that a realistic metabolic cost for normal human walking (~ 3.5 J/m/kg at ~ 1.3 m/s; Srinivasan, 2009) had the same weight in the cost function as a reasonably realistic average tracking error for these types of simulations (under ~ two standard deviations on average, e.g. Allen & Neptune, 2012; Miller, 2014).

The specific form of the muscle excitations function was:

$$J_{exc} = \frac{1}{2\cdot 78}\sum_{m=1}^{78}\left[(T_i^{on} - \tau_i^{on})^2 + \left(T_i^{off} - \tau_i^{off}\right)^2\right]$$

where T_i^{on} is the normalized time within the gait cycle (0-100%) when the excitation for muscle i turns on, T_i^{off} is the time when this muscle's excitation turns off, and τ_i^{on} and τ_i^{off} are mean on/off off times from indwelling EMG data during healthy adult gait (Sutherland, 2001). The weighting coefficient $w_2 = 50$ increased the cost function score by 0.125 (a very light penalty), 0.5, and 2.0 (a very heavy penalty) for average deviations of 5, 10, and 20% from the normative timing data.

REFERENCES

Allen, J. L., Neptune, R. R., 2012. Three-dimensional modular control of human walking. Journal of Biomechanics 45, 2157-2163.

Miller, R. H., 2014. A comparison of muscle energy models for simulating human walking in three dimensions. Journal of Biomechanics 47, 1373-1381.

Miller, R. H., Edwards, W. B., Brandon, S. C., Morton, A. M., Deluzio, K. J., 2014. Why don't most runners get knee osteoarthritis? A case for per-unit-distance loads. Medicine and Science in Sports and Exercise 46, 572-579.

Miller, R. H., Esterson, A. Y., Shim, J. K., 2015. Joint contact forces when minimizing the external knee adduction moment by gait modification: A computer simulation study. The Knee 22, 481-489

Srinivasan, M., 2009. Optimal speeds for walking and running, and walking on a moving walkway. Chaos 19, 026112.

Sutherland, D.H., 2001. The evolution of clinical gait analysis part 1: kinesiological EMG. Gait and Posture 14, 61-70.

Tucker, V. A., 1975. The energy cost of moving about. American Scientist 63, 413-419.

Umberger, B. R., Gerritsen, K. G., Martin, P. E., 2003. A model of human muscle energy expenditure. Computer Methods in Biomechanics and Biomedical Engineering 6, 99-111.

Waters, R. L., Mulroy, S., 1999. The energy expenditure of normal and pathologic gait. Gait & Posture 9, 207-231.